Diversification of MgO//Mg interfacial crystal orientations during oxidation: A density functional theory study

Wenwu Xu[1,2], Andrew P. Horsfield[3*], David Wearing[3], and Peter D. Lee[1,2†]

[1]Manchester X-ray Imaging Facility, University of Manchester, Manchester M13 9PL, UK

[2]Research Complex at Harwell, Didcot OX11 0FA, UK

[3]Department of Materials, Imperial College London, London SW7 2AZ, UK

[*]a.horsfield@imperial.ac.uk; Tel(Fax): +44 20 7594 6753(7)

[†]peter.lee@manchester.ac.uk; Tel: +44 12 3556 7789

Abstract

In this work we use computer simulations to explain the variety of crystal orientations observed at interfaces between MgO and Mg when Mg single crystals are oxidized. Using first-principles density functional theory simulations we investigate the interfacial stability of MgO//Mg interfaces, and find that a combination of interfacial chemical bonding energy and epitaxial strain stored in the oxide layers can change the relative stability of competing MgO//Mg interfaces. We propose that a combination of the oxygen chemical potential at the interface plane and the epitaxial strain energy stored in the oxide layers is responsible for the differences in observed interfacial crystal orientations - a key insight for the design and development of Mg alloys reinforced by MgO particles.

Key words: interfacial stability; interfacial free energy; density functional theory; MgO//Mg interface.

1. Introduction

Magnesium and its alloys are attractive for use in lightweight structural systems, most notably automotive systems [1], where a low weight leads to increased fuel efficiency. However, the extremely high affinity of Mg to oxygen makes it prone to oxidation. This particular phenomenon can be beneficial if used to form a protective oxide film at the surface that increases the corrosion resistance of Mg-based alloys. When an oxide layer is grown upon a flat Mg crystal surface under ideal growth conditions [2], it is possible to form oxide films ranging from a monolayer up to ~10-20 Å (equivalent to <~5-10 atomic layers) [3]. The strain energy increases in proportion to the oxide thickness, until the oxide layers eventually find a way (e.g. by introduction of a dislocation [4]) to release the stress [5]. What remains unclear in this process is the formation mechanism of the interfacial crystal orientation relationships (ORs) between the oxides and the metal crystals, i.e. the relative stability of MgO//Mg interfaces. For example, a large number of experiments have focused on the oxidation of Mg(0001) which is the most stable surface of Mg, having the lowest surface free energy [6]. Various crystal ORs of the MgO//Mg interface have been observed by low energy electron diffraction (LEED) and high resolution transmission electron microscopy (HRTEM), as summarized in Table 1. Hayden et al. [7] observed the OR of MgO(100)//Mg(0001) from the surface oxidation of Mg(0001) single crystals and Kooi et al. [8] identified the same OR from the oxidation of Mg(0001) nanocrystals. In contrast, Namba et al. [9] and Flodström et al. [10] both reported the OR of MgO(111)//Mg(0001) resulting from the oxidation of the Mg(0001) surface. Zheng et al. [11] discovered the OR of MgO(110)//Mg(0001) by oxidizing the nanopores which were drilled by converged electron beam irradiation on a Mg(0001)

single crystal surface. Thus, there is strong evidence that the formation of the interfacial OR during oxidation is sensitive to the experimental conditions, particularly the preparation of the metal crystal surfaces as well as to the growth conditions of the oxides.

In most cases the formation and growth of oxide layers on metal crystal surfaces involves lattice mismatch between oxides and metal crystals, which induces epitaxial strain in the oxide layers. Note that we assume here that the metal is much thicker than the oxide, hence only the oxide undergoes strain. Thus there are at least two major factors controlling the interfacial energy ($\gamma = \gamma_{ch} + \mu_{st}$), and hence the formation and/or growth of oxide layers on metal crystal surfaces: 1) the interfacial chemical bonding energy (γ_{ch}) and 2) the epitaxial strain energy (μ_{st}) stored in the oxide layers. A quantitative understanding of how atomic structure and interfacial free energy are related to the stability of interfaces between oxides and metal crystals is the key to revealing the mechanism of the formation and growth of oxides on metal crystal surfaces.

We present here an atomistic study of MgO//Mg interfaces to investigate the interfacial stability between Mg oxide and the Mg crystal surfaces. Density functional theory (DFT) offers a robust way to compute both the energies and structures of solid-state interfaces at the atomic level [12]. Hence, we employ DFT to simulate the atomic structures of the MgO//Mg interfaces and compute their interfacial free energies at the ground state (0 K). Our findings suggest that the combination of chemical bonding at the interface plane, including a contribution from the oxygen chemical potential, and the epitaxial strain in the oxide layers can change the relative stability of the various MgO//Mg interfaces, and thus could be responsible for the formation of the different ORs observed during oxidation of Mg. Furthermore, this work provides fundamental

knowledge relevant to the design and development of Mg alloys reinforced by MgO (nano)particles – an important metal matrix (nano)composite material [13, 14].

Table 1. Experimental crystal orientation relationships (ORs) of MgO(*hkl*)//Mg(*hkjl*) interfaces under different oxidation conditions.

ORs	MgO(*hkl*)//Mg(*hkjl*)		$[uvw]_{MgO}$//$[uvtw]_{Mg}$		Morphology of Mg(0001)
A	(100)	(0001)	[110]	[11-20]	single crystal [7]; nanocrystal [8]
B	(110)	(0001)	[001]	[11-20]	nanopore [11]
C	(111)	(0001)	[01-1]	[1-210]	single crystal [9, 10]

2. Theory

To develop our theory of the relative stabilities of the MgO//Mg interfaces, we consider the formation of a thin strained layer of MgO on a thick (and hence unstrained) slab of Mg crystal. As illustrated in Fig. 1, the oxidation reaction involves the removal of an Mg//O_2 interface, and the creation of MgO and two new interfaces: MgO//O_2 and Mg//MgO.

Before the reaction, the free energy of the system ($G^{(1)}$) is given by

$$G^{(1)} = N_{O_2}^{(1)}\mu_{O_2} + N_{Mg}^{(1)}\mu_{Mg} + s_{int}\gamma_{Mg//O_2} \quad (1)$$

where $N_{O_2}^{(1)}$ and $N_{Mg}^{(1)}$ are the number of O_2 molecules and Mg atoms respectively, and μ_{O_2} and μ_{Mg} are the corresponding chemical potentials. The quantity $\gamma_{Mg//O_2}$ is the Mg surface energy and s_{int} is the area of the interface.

After the reaction the free energy is $G^{(2)}$, which is given by

$$G^{(2)} = N_{O_2}^{(2)}\mu_{O_2} + N_{Mg}^{(2)}\mu_{Mg} + N_{MgO}^{(2)}\mu_{MgO} + \Delta N_O^{(2)}\mu_O + s_{int}(\gamma_{MgO//O_2} + \gamma_{MgO//Mg}) \quad (2)$$

where $N_{O_2}^{(2)}$ and $N_{Mg}^{(2)}$ are the number of O_2 molecules and Mg atoms respectively, and $\Delta N_O^{(2)}$ is the number of excess oxygen atoms at the MgO//Mg interface (this would be negative for a Mg rich interface, and zero when there is no excess of O or Mg atoms), and μ_{O_2}, μ_{Mg}, μ_O are the corresponding chemical potentials. The quantities $\gamma_{MgO//O_2}$ and $\gamma_{MgO//Mg}$ are the MgO//O_2 and MgO//Mg interfacial energies. It should be noted that $\gamma_{MgO//Mg}$ accounts only for the interfacial chemical bonding energy (the strain contribution is not included), we thus denote it as γ_{ch}, as mentioned in Section 1. Finally, μ_{MgO} is the chemical potential for strained MgO, and is where the strain energy is accounted for.

The conservation of mass yields the following equations

$$N_{O_2}^{(1)} = N_{O_2}^{(2)} + \frac{1}{2}\left(N_{MgO}^{(2)} + \Delta N_O^{(2)}\right) \quad (3a)$$

$$N_{Mg}^{(1)} = N_{Mg}^{(2)} + N_{MgO}^{(2)} \quad (3b)$$

Subtracting Eq. (1) from Eq. (2) and then substituting in Eq. (3) gives

$$\Delta G = G^{(2)} - G^{(1)} = N_{MgO}^{(2)}\Delta\mu_{MgO} + \Delta N_O^{(2)}\Delta\mu_O + s_{int}\Delta\gamma_{ch} \quad (4)$$

where

$$\Delta\mu_{MgO} = \mu_{MgO} - \mu_{Mg} - \frac{1}{2}\mu_{O_2} \quad (5)$$

$$\Delta\mu_O = \mu_O - \frac{1}{2}\mu_{O_2} \quad (6)$$

$$\Delta\gamma_{ch} = (\gamma_{MgO//O_2} + \gamma_{ch}) - \gamma_{Mg//O_2} \quad (7)$$

We take μ_{O_2} to be the chemical potential for gaseous oxygen molecules at equilibrium at a given temperature T and pressure P. Similarly, μ_{Mg} is taken as the chemical potential for bulk Mg metal, and μ_{MgO} that for strained bulk MgO. If the system were at equilibrium we would have to have the following relations between the chemical potentials be solved simultaneously: $\Delta\mu_O = 0$ and $\Delta\mu_O = \Delta\mu_{MgO}$. However, the system is not in equilibrium. In the present work, the interface system after oxidation (i.e. system 2 in Fig. 1) is assumed to be in a kinetically stabilized state, i.e. a metastable state, as described in Fig. 2, and the oxygen chemical potential and mobility might vary with distance from the outer surface. Because MgO can passivate an Mg surface, despite the thermodynamic driving force favouring continued oxidation, we assume there is a low mobility of oxygen and magnesium in the oxide layers. This low mobility acts as a barrier between the air side of the system and the metal side. We note that $\Delta\mu_O = 0$ corresponds to an oxygen rich environment (e.g. at the MgO//O_2 interface), while $\Delta\mu_O = \Delta\mu_{MgO}$ holds when there is excess Mg (e.g. at the MgO//Mg interface). We treat these as limiting values, with the actual value at some intermediate point within the oxide layer lying between them. We thus have

$$\Delta\mu_{MgO} \leq \Delta\mu_O \leq 0 \quad (8)$$

To enable us to compare the relative stabilities of the competing interfaces, we now define a factor of relative stability (or formability factor), g, of the interface system

after oxidation (i.e. system 2 in Fig. 1) with respect to its precursor system that is before oxidation (system 1 in Fig. 1) according to Eq. (9):

$$g = \frac{\Delta G}{N_{MgO}^{(2)}} - \mu_{MgO}^{(0)} \quad (9)$$

where $\mu_{MgO}^{(0)}$ represents the chemical potential of bulk MgO in its equilibrium state (i.e. the unstrained or relaxed bulk MgO, in contrast to μ_{MgO} representing the chemical potential of strained bulk MgO). The smaller the value of g is, the more stable the corresponding interface system will be.

Substituting Eq. (4) into Eq. (9), we then have

$$g = \Delta\mu_{st} + \frac{\Delta N_O^{(2)}}{N_{MgO}^{(2)}}\Delta\mu_O + s_{int}\frac{\Delta\gamma_{ch}}{N_{MgO}^{(2)}} \quad (10a)$$

where $\Delta\mu_{st}$ (unit: eV/MgO) represents the epitaxial strain energy per formula unit of MgO stored in the oxide layers,

$$\Delta\mu_{st} = \mu_{MgO} - \mu_{MgO}^{(0)} \quad (10b)$$

From Eq. (10) we see that the relative stability g (or in other words, the formability of an oxide layer) containing a given amount of oxide ($N_{MgO}^{(2)}$) can vary with interface structure through several terms: the oxide chemical potential μ_{MgO} which will depend on the strain state of the oxide; the amount of excess oxygen $\Delta N_O^{(2)}$; the chemical potential of oxygen in the oxide $\Delta\mu_O$; and the interfacial energy change $\Delta\gamma_{ch}$. In the case of stoichiometric (SC) interfaces, when there is no excess O or Mg atoms at the MgO//Mg interface plane, we have $\Delta N_O^{(2)} = 0$, and Eq. (10) can be simplified to

$$g = \Delta\mu_{st} + s_{int}\frac{\Delta\gamma_{ch}}{N_{MgO}^{(2)}} \quad (11)$$

and there are now just two contributions: the strain energy and the interface chemical energy. Note that for thick enough oxide layers, the strain energy will always dominate.

3. Computational details

We can compute $\gamma_{MgO//O_2}$ and $\gamma_{Mg//O_2}$ in Eq. (7) straightforwardly provided we can take it in the limit of very low O_2 pressure, which we treat as a vacuum. In this case, we have

$$\gamma_{MgO//O_2} \approx \gamma_{MgO//vac} \quad (12a)$$

$$\gamma_{Mg//O_2} \approx \gamma_{Mg//vac} \quad (12b)$$

where $\gamma_{MgO//vac}$ and $\gamma_{Mg//vac}$ are the surface energy per unit area of the unstrained slab of MgO(*hkl*)//*vac* and Mg(hkjl)//*vac* respectively, formed by the cleavage of the corresponding DFT relaxed bulk phases of MgO and Mg, respectively. This neglects the change in surface energy from straining the slab, which will be small. It has been found in the literature that this energy difference is about one magnitude smaller than the value itself of the surface energy of an unstrained surface when the strain (lattice deformation) in the surface plane is only a few percentages [15]. Eq. (7) now changes to

$$\Delta\gamma_{ch} \approx (\gamma_{MgO//vac} + \gamma_{ch}) - \gamma_{Mg//vac} \quad (13)$$

The computation of γ_{ch} in Eq. (13) (i.e. the interfacial chemical bonding energy of MgO//Mg interfaces) is carried out using a slab geometry [16, 17]. Previously in the literature [18], a sharp interface between the ionic and the metallic components has been

observed from *ab initio* molecular dynamics simulations of the early oxidation stages of Mg(0001). We therefore model the MgO//Mg interfaces as an atomically sharp junction between two surface components that are cleaved from the corresponding bulk phases along certain crystal orientations. Based on the aforementioned experimental observations of ORs using LEED and HRTEM (Table 1) [7-11], we build atomic models of MgO(*hkl*), with (*hkl*) as (100), (110), or (111), interfaced with Mg(0001), their corresponding interface unit cells indicated by the dotted quadrilaterals in Fig. 3(a). In addition, we perform atomistic simulations of MgO(*hkl*)//Mg(10-10) interfaces; their atomic models are shown in Fig. 3(b). Interfaces involving Mg(10-10) have been chosen because Mg(10-10) possesses a relatively high surface energy amongst the low-indexed Mg(*hkjl*) surfaces [19, 20], and thus provides a useful contrast with Mg(0001). The surface oxidation of the Mg(10-10) single crystal has also been experimentally investigated using LEED [7]. On Fig. 3(a) & 3(b), the two directions of interface units are indicated by the X and Y arrows. Note that, in the case of MgO(111)//Mg, while interfaces with both O and Mg terminations of MgO are simulated, only the interface unit cells with an O termination at the interface plane are presented in Fig. 3. In total, we consider eight models of MgO(*hkl*)//Mg(*hkjl*) interfaces, as listed in Table 2.

Table 2. Summary of the eight interfacial slabs simulated by DFT and their strain and chemical bonding characteristics. Each slab comprises *n* atomic layers of Mg(*hkjl*) and *m* atomic layers of MgO(*hkl*), and forms either a stoichiometric (SC) or a non-stoichiometric (NON) MgO//Mg interfacial slab. The epitaxial strains (due to lattice mismatch) in the oxide layers, the chemical bonding energy, and the strain energy stored

in the oxide are all calculated at 0 K. Regarding the lattice mismatch at the interface, the oxide layers are stretched or compressed to accommodate the metal lattices, as denoted by '+' and '–', respectively.

Components of MgO//Mg interfacial slabs			Lattice mismatches in the oxide layers[(a)]		Chemical bonding energy, γ_{ch} (J/m^2)	Strain energy, γ_{st} (eV/MgO)
	*n*Mg(*hkjl*)	*m*MgO(*hkl*)	along X (%)	along Y (%)		
SC	5(0001)	5(100)	+8.14	-6.34	1.04 [1.20[(b)]]	0.166
SC	-	5(110)	+8.14	-0.65	1.98 [1.78[(b)]]	0.080
NON	-	13(111)$_O$	+8.14	+8.14	0 ~ 2.97 [0 ~ 4.85[(b)]]	0.218
NON	-	13(111)$_{Mg}$	+8.14	+8.14	0.82 ~ 6.05 [0.25 ~ 6.50[(b)]]	0.218
SC	8(10-10)	5(100)	+8.14	+4.55	1.06	0.113
SC	-	5(110)	+8.14	-1.42	1.24	0.078
NON	-	13(111)$_O$	+8.14	+0.60	0 ~ 3.93	0.087
NON	-	13(111)$_{Mg}$	+8.14	+0.60	1.40 ~ 7.01	0.087

[(a)]Lattice mismatches along X and Y direction are calculated by $[x_{Mg(hkjl)}-x_{MgO(hkj)}]/x_{MgO(hkj)}$ and $[y_{Mg(hkjl)}-y_{MgO(hkj)}]/y_{MgO(hkj)}$, respectively, where x and y represent the respective in-plane lattice constants of surface components along X and Y direction.

[(b)]Interfacial free energies at 0 K calculated by DFT with GGA [21].

We construct our interface computational cells so as to have identical atomic structure at the two interface planes between alternating slabs, ensuring the cell contains only one type of interface; see Fig. 2 in Ref. [22] for details. We choose this approach because it is more computationally efficient than having an interface slab geometry in which the alternating interface slabs are separated by vacuum [22]. We stretch/compress the MgO(*hkl*) lattice along the XY plane to accommodate the Mg(0001) or Mg(10-10) lattice, which themselves are obtained from the DFT relaxed Mg bulk phase. Thus we correctly represent the oxidation behaviour on Mg single crystals, during which the Mg lattice is almost invariant.

There are two types of interfaces listed in Table 2: stoichiometric (SC) and non-stoichiometric (NON). For SC interfaces, the chemical bonding contribution (strain independent) is calculated by [22]

$$\gamma_{ch}^{SC} = \frac{1}{2s_{int}}\left(E_{int}^{slab} - E_S^{Mg} - E_S^{MgO}\right) = \frac{1}{2s_{int}}\left(E_{int}^{slab} - N_{Mg}\mu_{Mg} - N_{MgO}\mu_{MgO}\right) \quad (14)$$

where s_{int} denotes the area of an interface and the factor of 2 accounts for the fact that there are two identical interfaces per computational cell. E_{int}^{slab} is the total energy of the interface slab. E_S^{Mg} and E_S^{MgO} are the respective total energy of supercell of phase Mg and MgO, under the same conditions as in the interface slab; thus it consists of the same lattice parameters and numbers of atoms as in the corresponding interface model, though the z-direction (perpendicular to the XY plane) of the supercell is allowed to relax. The total energy of supercell phase Mg can be simplified as $E_S^{Mg} = N_{Mg}\mu_{Mg}$ where N_{Mg} is the number of Mg atoms in the supercell and μ_{Mg} is the chemical potential computed as the total energy per atom of the relaxed bulk phase Mg. This simplification can be made because the Mg lattice in the interface unit is kept the same as that of the relaxed bulk phase. As a consequence, there is no strain energy contribution to the interfacial free energy from the Mg(*hkjl*) part of the interfacial slab.

The epitaxial strain energy (per formula unit of MgO) stored in the oxide layers, $\Delta\mu_{st}^{SC}$, can be obtained by Eq. (15), consistent with the definition by Eq. (10b):

$$\Delta\mu_{st}^{SC} = \frac{1}{N_{MgO}}\left(E_S^{MgO} - N_{MgO}\mu_{MgO}^0\right) = \mu_{MgO} - \mu_{MgO}^0 \quad (15)$$

where N_{MgO} is the number of formula MgO in the strained supercell, and μ_{MgO}^0 is computed as the total energy of the relaxed bulk phase of MgO.

For NON interfaces, the chemical bonding contribution to the interfacial free energy is calculated from [23]

$$\gamma_{ch}^{NON} = \frac{1}{s_{int}} E_{int}^{bind} + \gamma_{MgO(111)//vac}^{strain} + \gamma_{Mg(hkjl)//vac}^{strain}$$

$$\approx \frac{1}{s_{int}} E_{int}^{bind} + \gamma_{MgO(111)//vac} + \gamma_{Mg(hkjl)//vac} \quad (16)$$

where $\gamma_{MgO(111)//vac}^{strain}$ and $\gamma_{Mg(hkjl)//vac}^{strain}$ are the respective surface energy per unit area of the strained slabs. By neglecting the change in surface energy from straining the slab, γ_{ch}^{NON} is calculated according to $\gamma_{MgO(111)//vac}$ and $\gamma_{Mg(hkjl)//vac}$ which are the respective surface energy per unit area of the unstrained slab of MgO(111) and Mg(*hkjl*), formed by the cleavage of the corresponding DFT relaxed bulk phases of MgO and Mg along certain crystal orientations.

E_{int}^{bind} in Eq. (16) is the binding energy at the interface, which is obtained by [23]

$$E_{int}^{bind} = \frac{1}{2}\left(E_{int}^{slab} - E_{slab}^{strain,MgO(111)} - E_{slab}^{strain,Mg(hkjl)}\right) \quad (17)$$

where E_{int}^{slab} is the total energy of the interface slab, $E_{slab}^{strain,MgO(111)}$ and $E_{slab}^{strain,Mg(hkjl)}$ are the respective total energy of the strained surface slabs of MgO(111) and Mg(*hkjl*), both with lattice parameters fixed (but allowing z-direction relaxation) to that based on the DFT relaxed Mg bulk. A sufficiently large distance between alternating surface slabs, both strained and unstrained, to avoid artificial interaction of neighboring surfaces is achieved by inserting ~11 Å vacuum [22].

$\gamma_{Mg(hkjl)//vac}$ in Eq. (16) is derived from the difference in total energies calculated for a free surface slab of Mg(*hkjl*) and the bulk phase of Mg, while $\gamma_{MgO(111)//vac}$ is a function of the oxygen chemical potential, μ_O, and is calculated by [6, 21]

$$\gamma_{MgO(111)//vac} = \frac{1}{2s_{int}}\left[E_{slab}^{unstrain,MgO(111)} - N_{MgO}^{Mg}\mu_{MgO}^{0} + (N_{MgO}^{Mg} - N_{MgO}^{O})\mu_O\right] \quad (18)$$

where $E_{slab}^{unstrain,MgO(111)}$ is the total energy of an unstrained surface slab of MgO(111). N_{MgO}^{Mg} and N_{MgO}^{O} are the number of Mg and O atoms in the surface slab, respectively. The possible range of μ_O at the interface is given by Eq. (8). Combining Eqs. (16)-(18), we now obtain the strain-independent chemical bonding contribution to the interfacial free energy for NON interfaces. Note that both γ_{ch}^{NON} and E_{int}^{bind} should be independent of the thickness (direction perpendicular to the interface plane) of the computational cells.

We now describe a method to calculate the epitaxial strain energy in the oxide layers of NON interface unit cells. First we compute the total energies, $E_{int}^{slab}(m)$, of a series of interface unit cells, e.g. *m*MgO(111)$_O$//5Mg(0001), with *m*=7, 13, 19, and 25. The values for *m* are chosen to ensure that both interfaces in the slab are the same. We then compute the differences in total energy between slabs; i.e. $\Delta E_1 = E_{int}^{slab}(13) - E_{int}^{slab}(7)$, $\Delta E_2 = E_{int}^{slab}(19) - E_{int}^{slab}(13)$, and $\Delta E_3 = E_{int}^{slab}(25) - E_{int}^{slab}(19)$. These energy differences are actually the energy of a 6-layer block of alternating Mg and O atoms (i.e. 3 formula units of MgO). The average (epitaxial) strain energy per formula unit of MgO in the interface units is thus computed as $\overline{\gamma}_{st}^{NON} = \frac{1}{3}\sum_i(\Delta E_i - 3E_{bulk}^{MgO})$. Accordingly, we obtain ΔE_1 =0.174 eV/MgO, ΔE_2 =0.159 eV/MgO, and ΔE_3 =0.166 eV/MgO, which gives $\overline{\gamma}_{st}^{NON}$=0.166 eV/MgO for the MgO(111)$_O$//Mg(0001) interface. Similarly, we obtained the average epitaxial strain energies in the oxide layers of the other interfaces, whose results are summarized in Table 2.

All calculations in the current work are performed using the plane wave DFT code Cambridge Serial Total Energy Package (CASTEP) [24]. The Perdew-Burke-Ernzerhof

(PBE) functional [25] within the generalized gradient approximation (GGA) is used for calculating the exchange and correlation energy. Brillouin zone integration is performed using k-points on a Monkhorst-Pack grid [26], with a k-point mesh spacing of 0.04 $Å^{-1}$ being used for all the calculations, including bulks, surfaces and interfaces. Norm-conserving pseudo-potentials were used, and a plane-wave basis set energy cut-off of 35 Ha (Hartree energy) was employed. Self-consistent field (SCF) calculations were converged to 10^{-9} eV/atom for the total energy calculations. The Broyden-Fletcher-Goldfarb-Shannon (BFGS) algorithm [27] was applied to relax the atomic positions and cell vectors (unless specifically mentioned), under which the geometry optimizations were run until the atomic forces were below 0.001 eV/Å.

4. Results and discussions

We first carried out comprehensive convergence tests for the total energies of bulk phases and surface slabs with respect to the planewave energy cut-off and the electronic k-point sampling: energy changes are converged to the order of 0.01 eV/atom. We also determined the number of atomic layers of each component ($n_{\mathrm{Mg}(hkjl)}$ and $m_{\mathrm{MgO}(hkl)}$) in each interface unit, such that there is no significant interaction between neighbouring interfaces. The final calculated properties in this work are found to be converged to a degree measurable by experiments: ~0.01 J/m^2 for surface and interfacial energies and 0.001 Å for lattice constants. Details of the specific interface unit cells used for the computations of interfacial free energies are shown in Table 2.

The calculated (experimental) lattice constants and cohesive energies, E^{coh}, of Mg and MgO bulk phases are: a_{Mg} = 3.267 (3.209 [28]) Å, c_{Mg} = 5.264 (5.218 [28]) Å,

E_{Mg}^{coh} = 1.37 (1.51 [28]) eV/atom and a_{MgO} = 4.272 (4.211 [29]) Å, E_{MgO}^{coh} = 11.70 (10.30 [29]) eV/MgO. These results indicate that our calculations are in reasonable agreement with experiment. The interfacial free energies and the epitaxial strain energy stored in the oxide layers of each interface model (eight in total) at 0 K are then calculated, as shown in Table 2. The calculated interfacial free energies of MgO(*hkl*)//Mg(0001) show reasonable agreement with previously reported DFT calculations also performed using a PBE GGA functional. In the case of the NON interface models, calculation details of the relevant unstrained free surface energies (according to Eq. 18) as well as interfacial free energies (according to Eqs. 16-18) are described in the Supplemental Material [30].

Based on the results in Table 2, we now compute the factor of relative stability g for each MgO//Mg interface model. Fig. 4 shows g as a function of the number of strained atomic layers of MgO(*hkl*) on Mg(0001), where *hkl* = 100, 110, and 111. First of all, it is observed that g for the MgO(111)//Mg interface with O termination (dashed lines) at the interface plane is smaller than for Mg termination with a similar oxygen chemical potential at the interface plane. This suggests that, for a given O chemical potential, the $\mathrm{MgO(111)_O}$//Mg(0001) interface is more stable than the $\mathrm{MgO(111)_{Mg}}$//Mg(0001) one. This is probably due to the stronger interfacial chemical bonding between Mg and O, compared to Mg and Mg [21, 22].

From Fig 4(b) we find that, when the number of atomic layers of strained MgO is smaller than 9, the low limit of g for $\mathrm{MgO(111)_O}$//Mg(0001) (corresponding to $\Delta\mu_O = 0$ in the inequation 8) is lower than for the other interfaces. With decreasing O chemical potential at the interface plane (with limit value of $\Delta\mu_O = \Delta\mu_{MgO}$ in the inequation 8), g of $\mathrm{MgO(111)_O}$//Mg(0001) interface moving towards larger value until it is completely

above the solid blue line, at which case the MgO(100)//Mg(0001) interface becomes more stable. In the meantime, the number of atomic layers of strained oxide reduces quickly because the crossover point between red dashed line and blue solid line moves towards smaller values at the horizontal axis. In the case of Mg termination at the interface plane, MgO(100)//Mg(0001) is always the most stable interface. Additionally, it is observed that there is a relative stability change between $MgO(111)_{Mg}$//Mg(0001) interface (black short-dashed line) at its low limit value of g (corresponding to $\Delta\mu_O = \Delta\mu_{MgO}$) and MgO(110)//Mg(0001) interface (orange solid line) when the number of atomic layers of strain oxide is ~8. Therefore, we observed a relative stability change among different orientation relations of MgO//Mg interfaces due to the variation of oxygen chemical potential at the interface plane in combination with the change in strain energy stored in the oxide layers, which we think is an important reason responsible for the differences in experimentally observed interfacial crystal orientations of MgO//Mg interfaces. Based on the results in Fig. 4(a) and (b), it is able to compute the phase diagram of interfacial stabilities of various MgO(*hkl*)//Mg(0001) interfaces in terms of oxygen chemical potential ($\Delta\mu_O$) and the number of strained MgO layers, as the results shown in Fig. 4(c). The shaded area (above the solid line) in Fig. 4(c) represents where $MgO(111)_O$//Mg(0001) is the stable interface when Mg is oxidized. In the region below the solid line indicates MgO(100)//Mg(0001) is the stable interface of Mg oxidation.

It is also interesting to notice in the literature that Francis and Taylor [31] have revealed by first-principles approach, at the earliest stage of surface oxidation of a Mg(0001) single crystal (less than one layer of oxide coverage), oxygen atoms prefer to occupy subsurface sites just under the outermost atomic layer of metal and take the lattice

structure of the Mg(0001) metal crystal; this would result in a crystal orientation of MgO(111)//Mg(0001) at the interface [31], consistent with our results for the oxygen rich limit. They also found that the subsurface oxides of intermediate oxygen coverage undergo spinodal decomposition [31], indicating a metastable interfacial stability.

As discussed above, we have demonstrated an ordering change in the relative interfacial stability of the MgO(*hkl*)//Mg(0001) interfaces as a result of competition between chemical bonding at the interfaces and epitaxial strain energies in the oxide layers. This could be an important reason for the experimentally observed formation of various interfacial crystal orientations between MgO and Mg, when the Mg single crystal surface is oxidized. The different levels of interfacial oxygen chemical potential and/or strain energy stored in the oxide layers alter the relative interfacial stability between different ORs.

In this final section of the results we look at the factor of relative stability g of MgO(*hkl*)//Mg(10-10) with *hkl* = 100, 110, 111, as shown in Fig. 5. We see that the interfacial orientation of $MgO(111)_O$//Mg(10-10) (represented by the dashed red line) is preferential when the chemical potential oxygen atoms at the interface plane is close to its value in the gaseous state, i.e. $\Delta\mu_O = 0$. Otherwise, MgO(100)//Mg(10-10) (represented by the solid blue line) is the most stable interface when the oxygen chemical potential at the interface plane is negative enough (with a limiting value of $\Delta\mu_O = \Delta\mu_{MgO}$). Obviously, the oxygen chemical potential at the interface plane affects the interfacial stability. It is also noted that the two low limit lines (dashed and short-dashed) follow a rather similar trend as that for the two solids lines, as can be seen more clearly in Fig. 5(b). This suggests that the epitaxial strain energy in the case of MgO(*hkl*)//Mg(10-10)

interface does not strongly influence the relative stability between different interfacial orientations, which is somewhat different from that in the case for MgO(*hkl*)//Mg(0001) interface. This is due to the strain energy per formula of MgO for the MgO(111)//Mg(10-10) (0.087 eV/MgO) being much smaller than that for the MgO(111)//Mg(0001) (0.218 eV/MgO), as listed in Table 2. We have computed the stability phase diagram of MgO(*hkl*)//Mg(10-10) from the results shown in Fig. 5(a) and (b). The stable region of the $MgO(111)_O$//Mg(10-10) interface is represented by the shaded area above the solid line. It is interesting to note that the stable region of the $MgO(111)_O$//Mg(10-10) interface is much smaller than that for the $MgO(111)_O$//Mg(0001) when Mg is oxidized.

It should be noted that the DFT-calculated first interlayer distance (perpendicular to the interface) in the oxide at the interface plane of each model deviates by ~4-5% from that in bulk MgO. But, starting from the second layer from the interface, the interface has nearly no effect on the interlayer distance. This may result in different levels of epitaxial strain energy stored in the first layer of oxide compared with those layers further away from the interface planes, which would have an effect on the interfacial free energies and hence interfacial stability. However, we think this effect may be significant only if one layer of oxide is formed on the Mg single crystal surface, but is probably not critical when the strain energy contribution to the interfacial free energies from even a few atomic layers of oxides is considered.

4. Conclusions

We have investigated the interfacial stability of MgO//Mg interfaces by means of density functional theory simulations (PBE with GGA as implemented in CASTEP). We

proposed a so-called factor of relative stability (or interfacial formability) of interface with different crystal orientations. We then quantified influences of the chemical bonding energy and the epitaxial strain energy stored in oxide layers on the interfacial stability of eight MgO//Mg interface models: MgO(*hkl*)//Mg(0001) and MgO(*hkl*)//Mg(10-10) with (*hkl*) equal to (100), (110), and (111), for both Mg and O terminations of MgO(111). The combination of chemical bonding energy and the epitaxial strain energy stored in the oxide layers can change the relative stability of the various MgO//Mg interfaces, with the ranking of their stability being a strong function of oxygen chemical potential at the interface planes. We therefore conclude that the different interfacial oxygen chemical potential and/or epitaxial strain energy stored in the oxide layers are responsible for, and explain, the differences in observed interfacial crystal orientations in seemingly similar experiments.

If maximizing the stability of the oxide layer results in maximum resistance to corrosion, then these results suggest that the oxide layers that form on Mg should have the (001) orientation. We might also be tempted to make the layers as thick as possible, but this has to be weighed against the formation of misfit dislocations that might significantly increase diffusion rates through the oxide [32]. We have also only studied the stability of the oxide films in air (or vacuum). However, aqueous environments are usually important for corrosion; to investigate this, we would need to introduce a new interface (MgO//H_2O), and to consider the pH of the environment [33], which we leave to future work.

Acknowledgements

The authors wish to acknowledge financial support from the ExoMet Project (which is co-funded by the European Commission in the 7th Framework Programme, contract FP7-NMP3-LA-2012-280421, the European Space Agency, and by the individual partner organizations), the EPSRC (EP/I02249X/1) and the Research Complex at Harwell. This work made use of the facilities of N8 HPC provided and funded by the N8 consortium and EPSRC (Grant No.EP/K000225/1), and the Imperial College London High Performance Computing service. Data statement: The software and necessary information to repeat the calculations are detailed in methods, together with representative results.

References

[1]. T.M. Pollock, Science, 328 (2010) 986-987.

[2]. D.A. King, D.P. Woodruff, Growth and properties of ultrathin epitaxial layers, Elsevier, Amsterdam ; Oxford, 1997.

[3]. M.A. Barteau, X.D. Peng, Mater. Chem. Phys., 18 (1988) 425-443.

[4]. J.W. Matthews, A.E. Blakeslee, J. Cryst. Growth, 27 (1974) 118-125.

[5]. W. Pfeiler, Alloy Physics : A Comprehensive Reference, Wiley-VCH, Weinheim, 2007.

[6]. W.B. Zhang, B.Y. Tang, J. Phys. Chem. C, 112 (2008) 3327-3333.

[7]. B.E. Hayden, E. Schweizer, R. Kotz, A.M. Bradshaw, Surf. Sci., 111 (1981) 26-38.

[8]. B.J. Kooi, G. Palasantzas, J.T.M. De Hosson, Appl. Phys. Lett., 89 (2006).

[9]. H. Namba, J. Darville, J.M. Gilles, Surf. Sci., 108 (1981) 446-482.

[10]. S.A. Flodstrom, C.W.B. Martinsson, Surf. Sci., 118 (1982) 513-522.

[11]. H. Zheng, S.J. Wu, H.P. Sheng, C. Liu, Y. Liu, F. Cao, Z.C. Zhou, X.Z. Zhao, D.S. Zhao, J.B. Wang, Appl. Phys. Lett., 104 (2014).

[12]. N.M. Harrison, Comp. Mater. Sci., 187 (2003) 45-70.

[13]. C.S. Goh, M. Gupta, J. Wei, L.C. Lee, J. Compos. Mater., 41 (2007) 2325-2335.

[14]. Y. Wang, Z. Fan, X. Zhou, G.E. Thompson, Philos. Mag. Lett., 91 (2011) 516-529.

[15]. M. Benoit, C. Langlois, N. Combe, H. Tang, M.J. Casanove, Phys. Rev. B, 86 (2012) 075460.

[16]. J.S. Wang, A. Horsfield, U. Schwingenschlogl, P.D. Lee, Phys. Rev. B, 82 (2010) 184203.

[17]. J.S. Wang, A. Horsfield, P.D. Lee, P. Brommer, Phys. Rev. B, 82 (2010) 144203.

[18]. C. Bungaro, C. Noguera, P. Ballone, W. Kress, Phys. Rev. Lett., 79 (1997) 4433-4436.

[19]. S.Q. Huang, X.L. Zeng, X.H. Ju, S.Y. Xu, Adv. Mater. Res.-Switz, 554-556 (2012) 1609-1612.

[20]. J.J. Tang, X.B. Yang, L.Z. OuYang, M. Zhu, Y.J. Zhao, J. Phys. D: Appl. Phys., 47 (2014).

[21]. E.T. Dong, P. Shen, L.X. Shi, D. Zhang, Q.C. Jiang, J. Mater. Sci., 48 (2013) 6008-6017.

[22]. W.W. Xu, A.P. Horsfield, D. Wearing, P.D. Lee, J. Alloys Compd., (2015) 228-238.

[23]. S. Walter, F. Blobner, M. Krause, S. Mueller, K. Heinz, U. Starke, J. Phys.: Condens. Matter, 15 (2003) 5207-5221.

[24]. S.J. Clark, M.D. Segall, C.J. Pickard, P.J. Hasnip, M.J. Probert, K. Refson, M.C. Payne, Zeitschrift Fur Kristallographie, 220 (2005) 567-570.

[25]. J.P. Perdew, K. Burke, M. Ernzerhof, Phys. Rev. Lett., 77 (1996) 3865-3868.

[26]. H.J. Monkhorst, J.D. Pack, Phys. Rev. B, 13 (1976) 5188-5192.

[27]. B.G. Pfrommer, M. Cote, S.G. Louie, M.L. Cohen, J. Comput. Phys., 131 (1997) 233-240.

[28]. N.W. Ashcroft, N.D. Mermin, Solid State Physics, Holt, Rinehart and Winston, New York, 1976.

[29]. J. Goniakowski, C. Noguera, Phys. Rev. B, 60 (1999) 16120-16128.

[30]. See supplemental material at [URL will be inserted] for calculation details of surface and interfacial free energies of MgO(111)/Mg(*hkjl*) systems.

[31]. M.F. Francis, C.D. Taylor, Phys. Rev. B, 87 (2013) 075450.

[32]. I. Sakaguchi, H. Yurimoto, S. Sueno, Solid State Communications, 84 (1992) 889-893.

[33]. F. Tielens, C. Minot, Surface Science, 600 (2006) 357-365.

Figure captions:

Fig. 1. Cartoon of the oxidation reaction between Mg crystal and oxygen gas.

Fig. 2. Passivation effect of oxidation on Mg metal surface suggests a kinetically stabilized metastable interface system with certain thickness (typically ~10-20 nm) of MgO layer between Mg metal and Air.

Fig. 3. Schematic diagrams of atomic models of interfaces used for DFT simulations: (a) MgO(*hkl*)//Mg(0001); (b) MgO(*hkl*)//Mg(10-10). (*hkl*) includes (100), (110), and (111). The interface unit cells with various crystal orientations are indicated by dotted lines. The two directions of interface units are indexed with X and Y. In the case of MgO(111)//Mg only the O termination at the interface plane is presented.

Fig. 4. (a) *g* as a function of the number of atomic layers of strained MgO for each interface model of MgO(*hkl*)//Mg(0001) with *hkl* = 100, 110, 111; (b) local enlargement of (a) indexed by blue dotted box; (c) stability phase diagram of MgO(*hkl*)//Mg(0001) interfaces. For O termination interfaces, the low and high limit values of *g* correspond to $\Delta\mu_O=0$ and $\Delta\mu_O=\Delta\mu_{MgO}$, respectively. Whereas for Mg termination interfaces, the low and high limit values of *g* correspond to $\Delta\mu_O=\Delta\mu_{MgO}$ and $\Delta\mu_O=0$, respectively.

Fig. 5. (a) *g* as a function of the number of atomic layers of strained MgO for each interface model of MgO(*hkl*)//Mg(10-10) with *hkl* = 100, 110, 111; (b) local enlargement of (a) indexed by blue dotted box; (c) stability phase diagram of MgO(*hkl*)//Mg(10-10) interfaces. For O termination interfaces, the low and high limit values of *g* correspond to $\Delta\mu_O=0$ and $\Delta\mu_O=\Delta\mu_{MgO}$, respectively. Whereas for Mg termination interfaces, the low and high limit values of *g* correspond to $\Delta\mu_O=\Delta\mu_{MgO}$ and $\Delta\mu_O=0$, respectively.

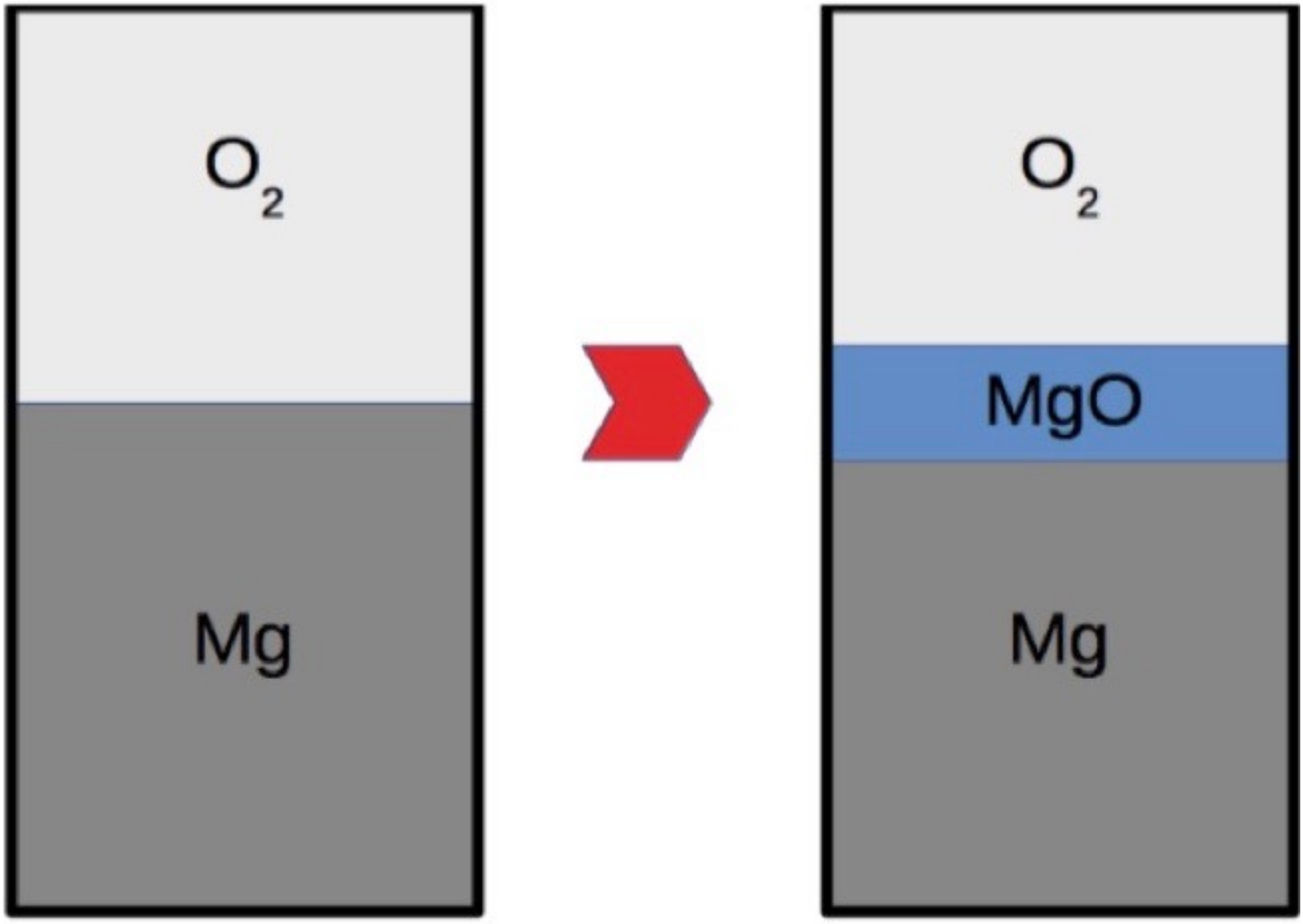

System 1

System 2

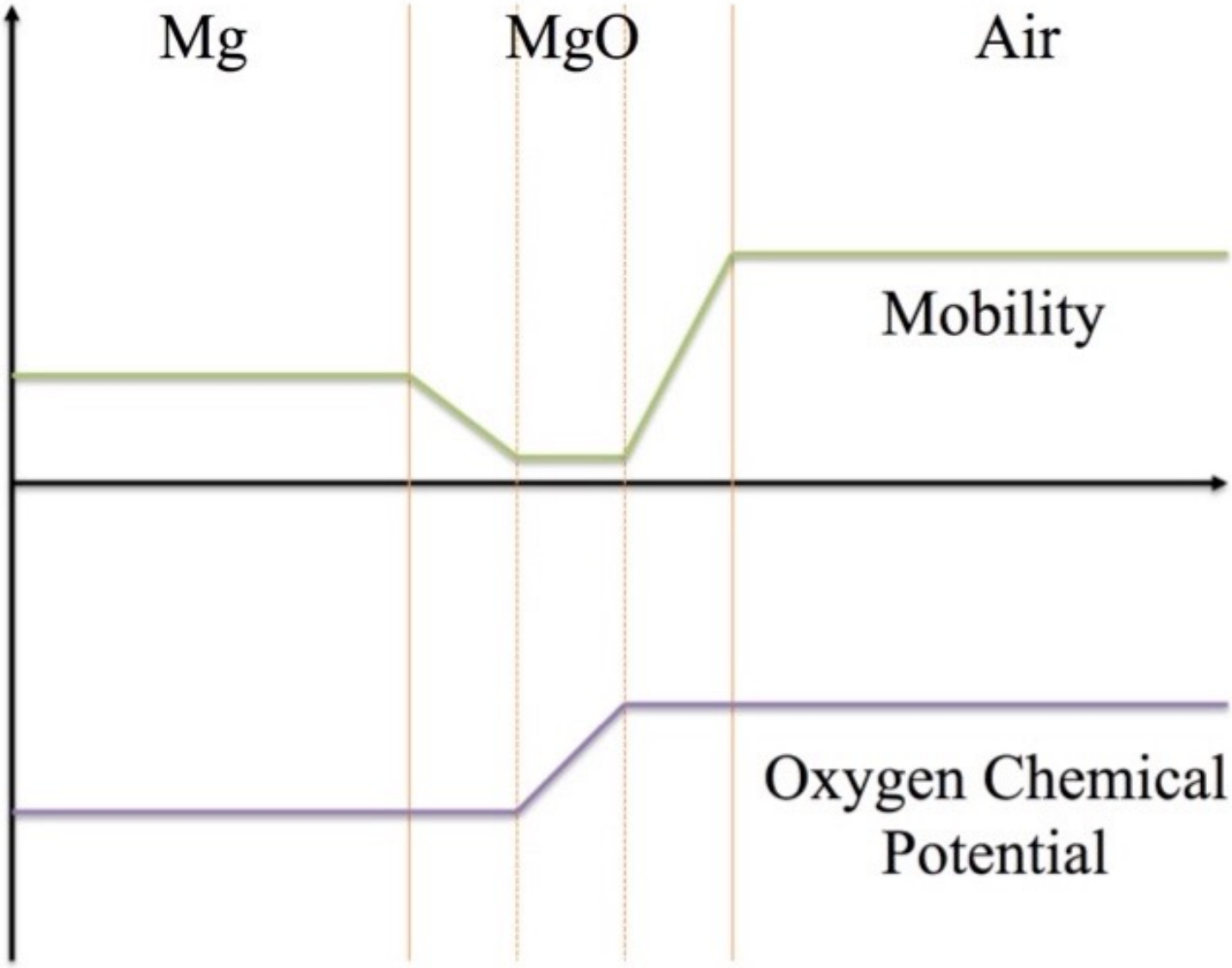
Mg
MgO
Air
Mobility
Oxygen Chemical Potential

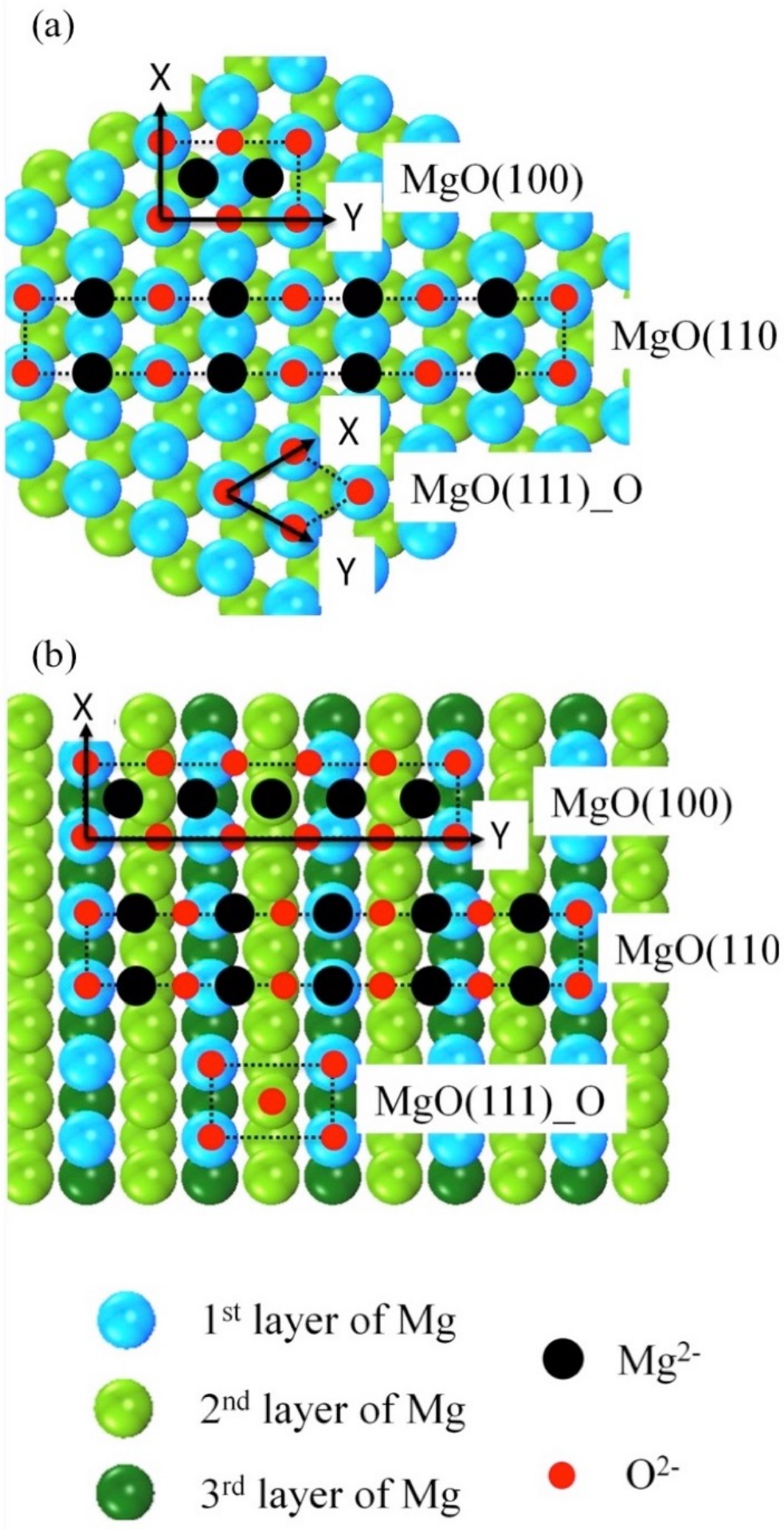
(a)
X
Y
MgO(100)
MgO(110
X
Y
MgO(111)_O
(b)
X
Y
MgO(100)
MgO(110
MgO(111)_O
1st layer of Mg
2nd layer of Mg
3rd layer of Mg
Mg2-
O2-

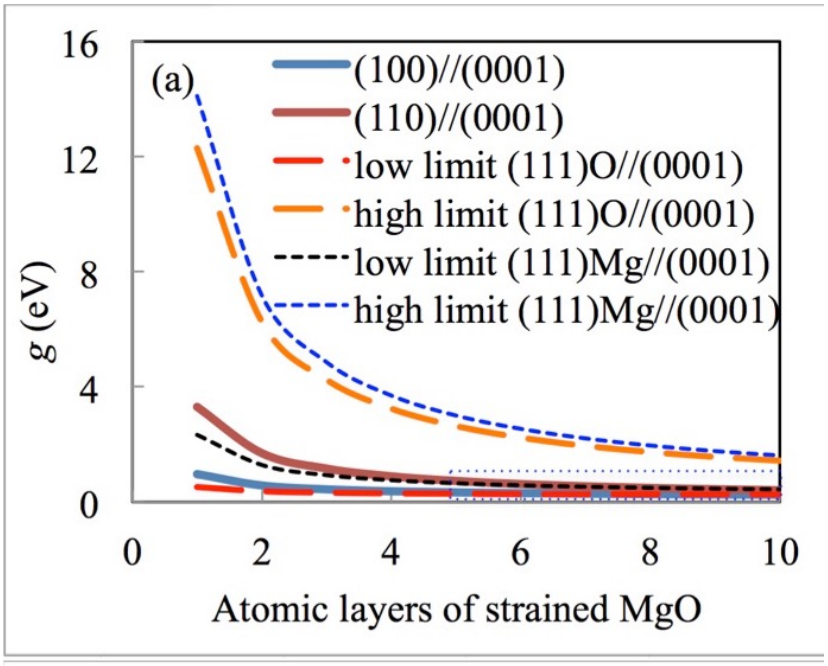
(a)
(100)//(0001)
(110)//(0001)
low limit (111)O//(0001)
high limit (111)O//(0001)
low limit (111)Mg//(0001)
high limit (111)Mg//(0001)
g (eV)
16
12
8
4
0
0
2
4
6
8
10
Atomic layers of strained MgO

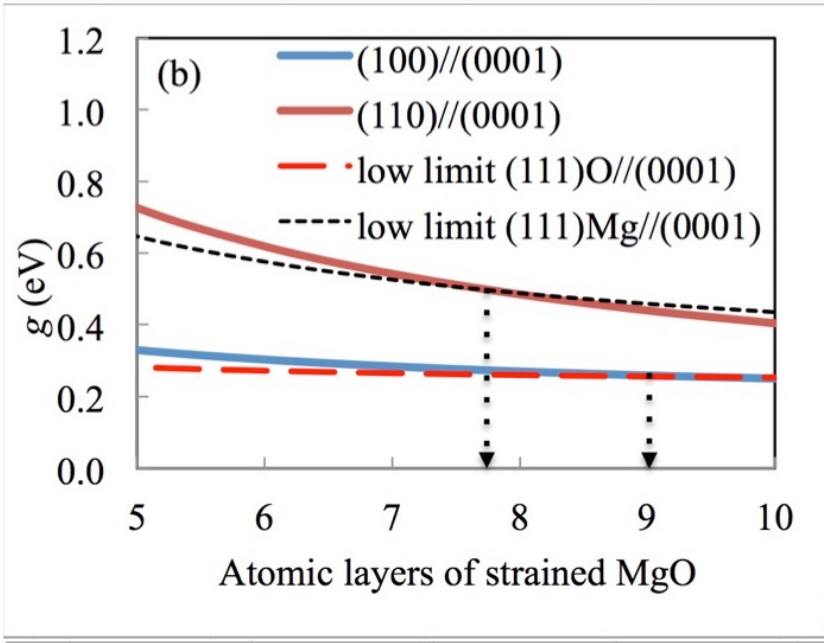
(b)
(100)//(0001)
(110)//(0001)
low limit (111)O//(0001)
low limit (111)Mg//(0001)
g (eV)
1.2
1.0
0.8
0.6
0.4
0.2
0.0
5
6
7
8
9
10
Atomic layers of strained MgO

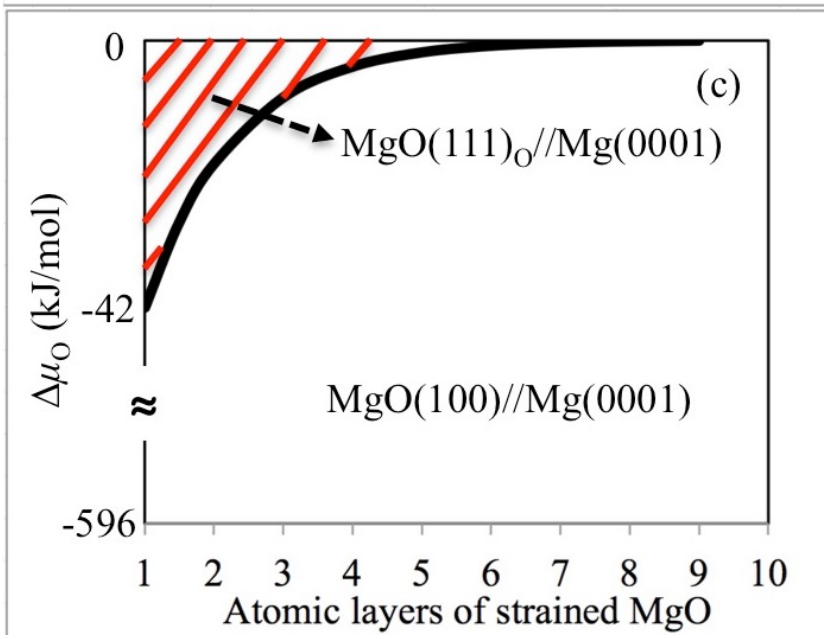
(c)
MgO(111)O//Mg(0001)
MgO(100)//Mg(0001)
Δμ_O (kJ/mol)
0
-42
-596
1
2
3
4
5
6
7
8
9
10
Atomic layers of strained MgO

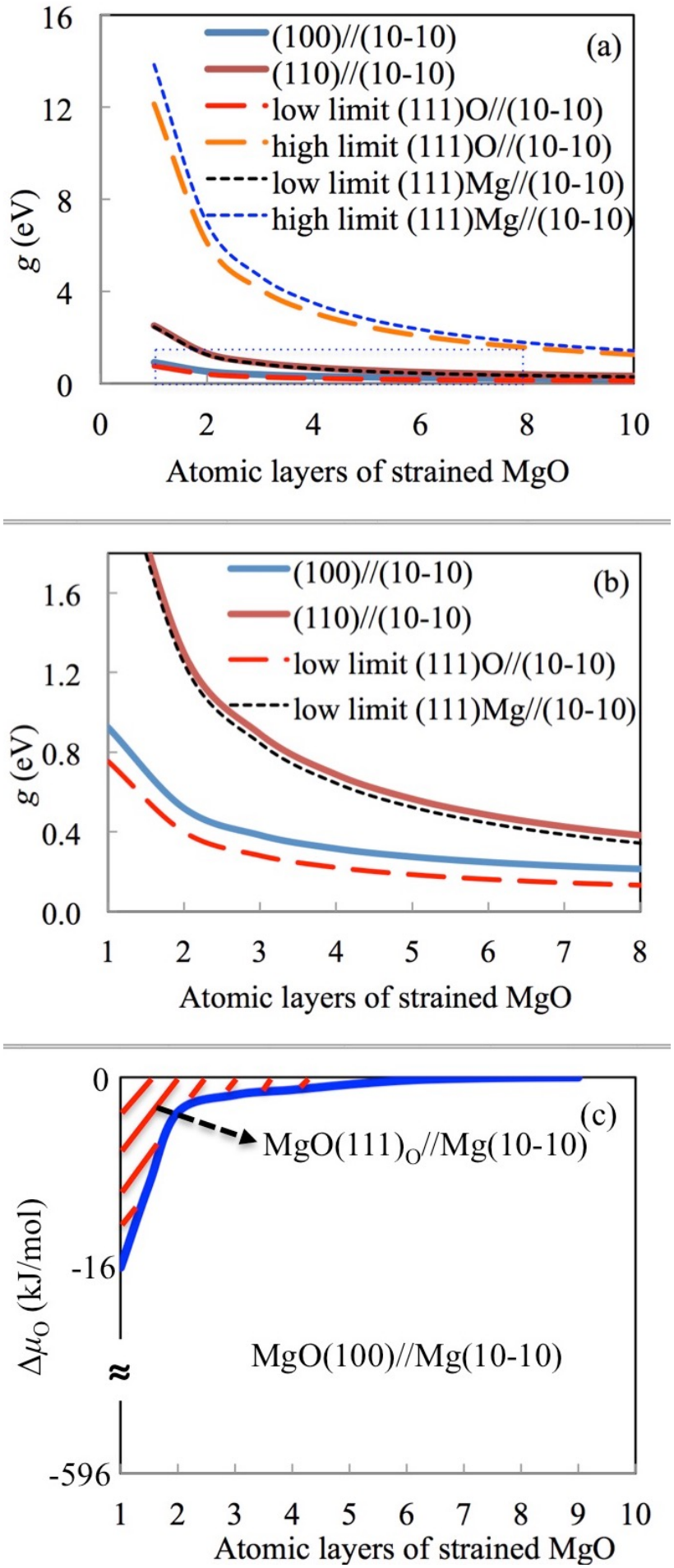
(a)
(100)//(10-10)
(110)//(10-10)
low limit (111)O//(10-10)
high limit (111)O//(10-10)
low limit (111)Mg//(10-10)
high limit (111)Mg//(10-10)
g (eV)
Atomic layers of strained MgO
(b)
(100)//(10-10)
(110)//(10-10)
low limit (111)O//(10-10)
low limit (111)Mg//(10-10)
g (eV)
Atomic layers of strained MgO
(c)
MgO(111)O//Mg(10-10)
MgO(100)//Mg(10-10)
Δμ_O (kJ/mol)
Atomic layers of strained MgO